Accepted Article

This manuscript has been accepted after peer review and appears as an Accepted Article online prior to editing, proofing, and formal publication of the final Version of Record (VoR). This work is currently citable by using the Digital Object Identifier (DOI) given below. The VoR will be published online in Early View as soon as possible and may be different to this Accepted Article as a result of editing. Readers should obtain the VoR from the journal website shown below when it is published to ensure accuracy of information. The authors are responsible for the content of this Accepted Article.

WILEY-VCH

COMMUNICATION

Zerovalent Rh and Ir Silatranes Featuring 2-center, 3-electron Polar Sigma Bonds

Patricia J. Nance, Niklas B. Thompson, Paul H. Oyala, and Jonas C. Peters*

Dedication

Abstract: *Species with 2-center, 3-electron (2c/3e⁻) -bonds are of interest owing to their fascinating electronic structures and potential for interesting reactivity patterns. Herein we report the synthesis and characterization of a pair of zerovalent (d⁹) trigonal pyramidal Rh and Ir complexes that feature 2c/3e⁻ -bonds to the Si atom of a tripodal tris(phosphine)silatrane ligand. X-ray diffraction, continuous wave and pulse electron paramagnetic resonance, density functional theory calculations, and reactivity studies have been used to characterize these electronically distinctive compounds. The data available highlight a 2c/3e⁻ bonding framework with a *-SOMO of metal 4- or 5d$_z$² parentage that is partially stabilized by significant mixing with Si (3p$_z$) and metal (5- or 6p$_z$) orbitals. Metal-ligand covalency thus buffers the expected destabilization of transition metal (TM)-silyl *-orbitals via d. p mixing, affording well-characterized examples of TM-to-main group, and hence polar, 2c/3e⁻ ‰@¦-bonds+*

First proposed by Linus Pauling almost a century ago, two-center, three-electron (2c/3e⁻) -bonds are still rarely observed. The &¦æ•ﺏÁ^¢æ¦]¦^Á[-Áɾ@•^^Á¸ ^æÁ‰@¢¦-à[} å•+Áã Á-{ }åÁã¸Áɾ@Á metastable He₂⁺ ﺏ¦ } Ě¸ @&@Ǎ˘•^•Á¸ [Á^¦^&d[} Á¦¸ÁæÁ -bonding [¦à¾æ¦Áæﻥ åÁæ¾Á@¾åÁ^¦^&d[} Á¦¸ÁæÁ -antibonding orbital.[1] Over the years, a limited number of other examples of 2c/3e⁻ bonds have arisen. For example, unsupported diatomic noble gas monocations and halogen monoanions have been spectroscopically characterized, and structurally characterized in the solid state in the case of Xe₂⁺.[2,3] Supported 2c/3e⁻ bonds have also been the subject of many experimental and theoretical studies, leading to the expansion of this bonding scheme to the pnictogen and chalcogen families (Figure 1a).[4,5,6,7,8] With respect to 2c/3e⁻ bonds featuring a transition metal (TM), bona fide examples of these bonds have been reported in a fascinating class of homobimetallic, mixed valence Ni₂(II,III) and Pd₂(II,III) paddlewheel complexes, as well as several Fe and Co piano stool dimers.[9,10,11]

Following the spectroscopic characterization of a boron-boron one-^¦^&d[} Á -bond (Figure 1b),[12] our group later reported on a copper-boratrane complex featuring a polar Cu. B 2c/1e⁻ -bond, the first of its type with a TM center (Figure 1b).[13,14] Herein, we describe the extension of this approach towards well-defined 2c/3e⁻ TM. E -half-bonded complexes featuring a TM (Rh or Ir) and a main group element E (Si).[15] Specifically, we report the thorough characterization of zerovalent, d⁹ Rh and Ir complexes [K(THF)₃][P₃^{Si}M] (M = Rh, Ir; P₃^{Si} = tris(o-diisopropylphosphinophenyl)silylide) (Scheme 1). Electron paramagnetic resonance (EPR), density functional theory (DFT) calculations and X-ray structural characterization data highlight

[*]   P. J. Nance, Dr. N. B. Thompson, Dr. P. H. Oyala, Prof. Dr. J. C.
        Peters
        Division of Chemistry and Chemical Engineering
        California Institute of Technology
        Pasadena CA 91125 (USA)
        E-mail: jpeters@caltech.edu

        Supporting information for this article is given via a link at the end of
        the document.

their fascinating electronic structures. In particular, the highest-¦^ﺏ * Á EÂÙUT UÁ -¸@¯Á&&Đ¹^¯ bond framework is partially stabilized by significant mixing of the 3p$_z$ orbital on the silicon atom of the silatrane ligand with a lobe of metal 4- or 5d$_z$² parentage. This mixing is manifest via pulse EPR studies.

Figure 1. Select examples of supported a) 2-center, 3-electron (**N** = N-(*p*-methoxyphenyl)) and b) 2-center, 1-electron -bonds. See text.

One-electron reduction of the previously reported precursors P₃^{Si}M(N₂) (M = Rh (**1**), Ir (**2**)) (Scheme 1)[16,17] æ¸Á Ì Ì ÁÔÁæ-{ ¦å¸ÁÁ access to the zerovalent [K(THF)₃][P₃^{Si}Rh] (**3**) and [K(THF)₃][P₃^{Si}Ir] (**4**) complexes of interest. The cyclic voltammograms of **1** and **2** show quasireversible reduction waves æ¸Á HÈ¸Áæ¦ åÁ HÈ¸ÁŐ• ĐŽ&ĐŽ&⁺, respectively, necessitating the use of potassium graphite or potassium naphthalenide as the reductant (see SI). Perhaps unsurprisingly, addition of an electron into the 18-electron precursors **1** and **2** causes dissociation of the N₂ ligand. Zerovalent Rh and Ir complexes are rather rare, especially for isolable examples.[18,19,20,21]

Scheme 1. Synthesis of Rh and Ir complexes **3**-**6**.

Samples of **3** and **4** suitable for X-ray diffraction (XRD) were prepared via recrystallization from a concentrated THF solution layered with chilled pentane, •¢¦^åﻥæ¸Á HÉ¸Á¸ÔÊV@ir solid-state structures, which are shown in Figure 2, were solved in a trigonal crystal system that imposes three equivalent M. P bond distances along with C_3 symmetry about the Si. M. K axis. This symmetry agrees with the symmetry observed in solution via

COMMUNICATION

spectroscopy (*vide infra*). The trigonal pyramidal geometry of **3** and **4** is distinctive among the limited number of known zerovalent Rh and Ir complexes, most of which have D_{2d} symmetry.[18,19,20,21,22] For both **3** and **4**, the dihedral angle between the planes formed by P1. M. P2 and P3. M. Ù̀ãɓ̀ ÁJ €»Áɓ̀ àÁ̀c@ Á₄ value is 86.7, thus showing only minor deviations from an ideal trigonal pyramidal geometry.[23] While the location of the K^+ cations in the solid-state is interesting to consider with respect to possible M. K interactions, such interactions can be easily ruled out *in solution* (see SI).
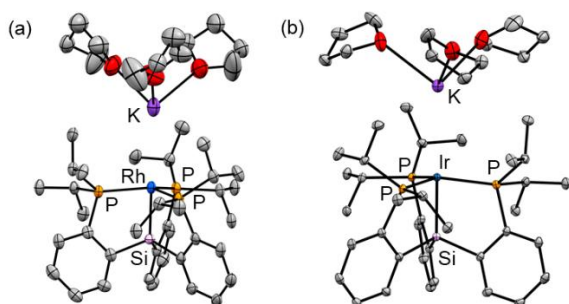
Figure 2. Solid state structures of Rh complex **3** (a) and Ir complex **4** (b). Thermal ellipsoids are depicted at 50% occupancy.

The 77 K X-band continuous wave (CW) EPR spectra of $[P_3^{Si}Rh]^-$ **3** and $[P_3^{Si}Ir]^-$ **4** each give rise to axial signals with $g_\perp > g_\parallel$ ($g_\perp$ is the more intense signal that corresponds to the xy plane of the molecule; $g_\parallel$ corresponds to the unique axis, z, oriented parallel to the M-Si bond vector) (Figure 3). Both complexes exhibit anisotropic hyperfine coupling to their corresponding metal nucleus, ^{29}Si, and three equivalent ^{31}P nuclei, implying that the C_3 symmetry observed by XRD is maintained in solution. Metalloradical character is evidenced in the *g* anisotropy (*g*) observed for **3** and **4**, which is larger in the case of the Ir analogue. An increase in metalloradical character is to be expected when moving to a third-row transition metal, as the ligand orbitals mix less with the metal d-orbitals due to poorer energetic overlap that is not sufficiently compensated by increased orbital overlap. In this case, the reduced metal-ligand covalency of **4** should translate to greater localization of the SOMO on the metal center. The large magnitude of the increase in *g* can also be attributed to the greater spin-orbit coupling of Ir.[24]
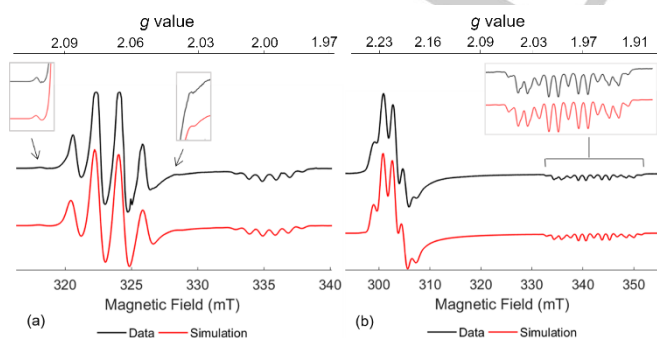
Figure 3. CW X-band EPR spectra at 77 K and corresponding simulations of (a) Rh complex **3** and (b) Ir complex **4**. Insets show (a) satellite peaks and (b) shoulders resulting from ^{29}Si hyperfine coupling.

Table 1. EPR Parameters for Complexes 3 and 4[a]

	Complex	g_x	g_y	g_z
Value	Rh	2.075	2.075	2.000
	Ir	2.208	2.214	1.957
g	Rh	0.075	.	.
	Ir	0.25	.	.
$A(^{31}P)^b$	Rh	52	52	28.5
	Ir	60	60	40
$A(^{29}Si)$	Rh	140	140	170
	Ir	114	114	136
$A(^{103}Rh)$	.	7	7	53
$A(^{191/193}Ir)$	.	20	20	130.5

[a]Hyperfine coupling constants are in MHz. [b]All three ^{31}P nuclei are equivalent.

As an additional tool to probe their electronic structures, Davies electron-nuclear double resonance (ENDOR) spectra were acquired at X-band frequencies (~9.7 GHz) for **3** at 20 K and **4** at 12 K. These data enabled the determination of the ^{31}P, ^{103}Rh, and $^{191/193}Ir$ hyperfine tensors (Table 1). Furthermore, we find that ^{29}Si hyperfine coupling values can be extracted from the ENDOR spectra, which to our knowledge is the first example of such characterization applied to a TM-silyl complex (Figure 4). Corresponding simulations were constrained by fitting the CW X-band spectra of each complex. For both complexes, all coupled nuclei show doublets that are centered at *A*/2 and split by twice their nuclear Larmor frequency (~6 MHz for Si, ~12 MHz for P, <1 MHz for Rh and Ir at X band frequencies), indicative of hyperfine couplings in the strong coupling limit ($A > 2*\nu_I$).[25] The large shift of the Rh and Ir ENDOR signals to higher frequencies as the *g*-value decreases from $g_\perp$ to $g_\parallel$ is suggestive of strong coupling along the principal axis due to the orientation of the spin density relative to the molecular frame. Additionally, hyperfine sublevel correlation (HYSCORE) spectroscopy shows weak coupling to natural abundance ^{13}C that indicates some delocalization of spin density onto the broader ligand platform through noncovalent spin polarization mechanisms (Figure 4, see SI for full data set). The hyperfine tensor associated with this natural abundance ^{13}C coupling was determined to be [3.2, 3.2, 5.8] MHz for **3** and [1.0, 1.0, 5.0] MHz for **4**.

The fact that hyperfine coupling to ^{29}Si (4.7% natural abundance) is sufficiently strong to observe satellite peaks and shoulders in the CW spectra (Figure 3, insets) and ^{29}Si signals in the ENDOR spectra suggests significant contribution of Si orbitals to the SOMOs of **3** and **4**. Decomposition of the ^{29}Si hyperfine tensor of **3** into its isotropic (a_{iso} = 1/3 ($A_x + A_y + A_z$) = 150 MHz) and anisotropic components ($T = [(A_x - a_{iso}), (A_y - a_{iso}), (A_z - a_{iso})]$) can be used to estimate the spin density residing in the Si 3s and $3p_z$ orbitals. This process reveals a fully axial anisotropic silicon hyperfine interaction with **T** M̌Ẑ F€̌Ả F€̌Ẑ€áT P: ̌ẢDefining the anisotropic tensor for an electron fully localized in a Si $3p_z$ orbital as T^0 M̌ẄFFI ̌ẢFFI ̌Ả GG̀ áT P: ̌Ẻ[26] spin density in the Si $3p_z$ orbital of **3** ã̀ Á[˘ } å̀Á[Å̀a^Á Å̀d̀ÁΕ̌ẺJÁ[¦̀ả̀J́Ã Á[-Å̀æ) Á^̀ |̀^&d̀ [} Ð̌Ẅ♦ ã̀ * Á̀a_{iso}^0 = 4594 MHz, the Si 3s character in the SOMO is found to be ~3.3%.[26] This analysis was carried out for ^{29}Si, ^{31}P, and the isotropic component of the metal hyperfine coupling and is
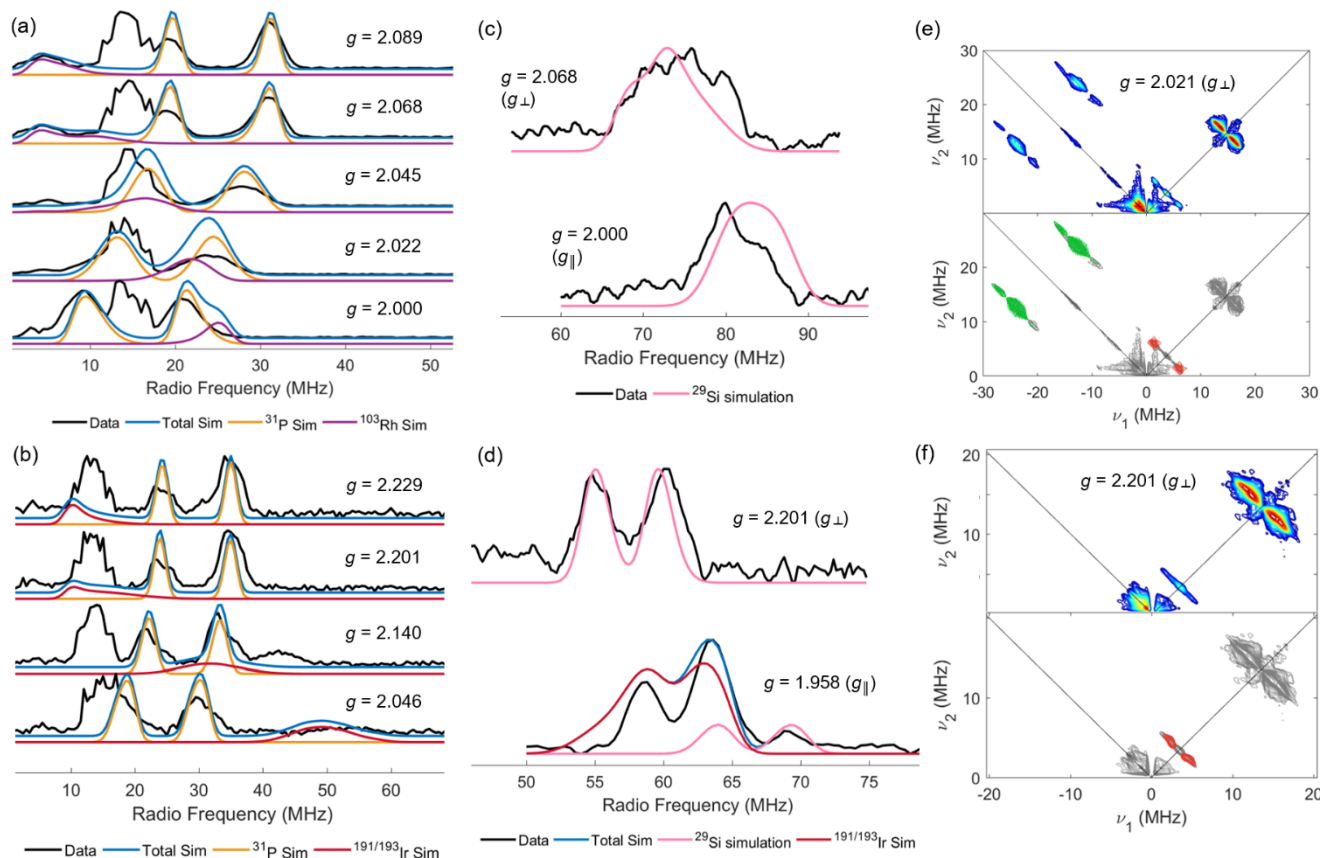
COMMUNICATION

Figure 4. Field-dependent X-band Davies ENDOR and corresponding simulations of (a) complex **3** and (b) complex **4** in the ^{31}P and transition metal coupling region; (c) complex **3** and (d) complex **4** in the ^{29}Si coupling region. (e) X-band HYSCORE spectrum of **3** at g = 2.021 (top) and and corresponding simulations (bottom, ^{31}P in green, ^{13}C in red). (f) X-band HYSCORE spectrum of **4** at g = 2.201 (top) and corresponding simulations (bottom, ^{13}C in red). See SI for experimental parameters

reported in Table 2. As this method cannot differentiate between spin density in p_z and d_{z^2} orbitals, which possess the same axial symmetry, the spin density estimate from the anisotropic component of the metal hyperfine tensor was not calculated.

DFT calculations (TPSSh, second-order DKH scalar relativistic treatment, cc-pVDZ-DK for all atoms except Ir, Si, and P, for which cc-pVTZ-DK was used; single-point calculation performed using nuclear coordinates from crystal structure) were employed to predict hyperfine tensors for the ^{29}Si and ^{31}P atoms of complex **4**. The total ^{29}Si tensor, A (^{29}Si), was calculated to be [137, 137, 159] MHz and A (^{31}P) was found to be [67, 64, 50] MHz. These values can be compared with those obtained from the CW EPR and ENDOR simulations (A (^{29}Si) = [114 114 136]; A (^{31}P) = [60 60 40]). The DFT-computed SOMO of **3** (Figure 5) has a_1 symmetry and nicely illustrates the mixing between the axially oriented Si and metal orbitals, as well as the antibonding nature of the interaction.[27] Calculated Löwdin spin populations (Table 2) show that the spin densities of **3** and **4** are primarily metal based (~50% of the unpaired spin on the metal atoms), but with significant delocalization onto the silicon and three equivalent phosphorus atoms. Löwdin reduced orbital spin population analysis quantifies the spin populations of participating orbitals; this shows that metal-based spin is primarily localized within axial orbitals (e.g. 4- or $5d_{z^2}$ and 5- or $6p_z$) with small isotropic components. The Si $3p_z$ orbitals accommodate most of the spin on Si, while the Si s orbital houses ~2% in both cases. The reduced orbital spin population

calculations for Si agree with the spin populations estimated from the breakdown of the experimental hyperfine tensors. As å^{ [}•dæˆåÁ¢] ^¦ā ^}æd¦ Áˆ Áˆ¢@ Á g values from the CW EPR, DFT calculations predict more metalloradical character for Ir complex **4** than **3**. The remaining ~20% of the spin density for both complexes is delocalized over the rest of the ligand, consistent with the observation of natural abundance ^{13}C signals in the HYSCORE data.

Table 2. Calculated Löwdin Spin Populations and Experimental Spin Density Estimations

	Rh DFT	Rh EPR[b]	Ir DFT	Ir EPR[b]
Metal	48	NC[c]	52	NC
s	5.4	1.8	3.6	1.6
p_z	25	NC	31	NC
d_{z^2}	18	NC	17	NC
^{29}Si	11	12	8.8	9.0
s	1.7	3.3	1.4	2.6
p_z	7.1	8.8	5.5	6.4
$^{31}P_1$[d]	6.7	2.5	4.3	2.2
s	0.057	0.33	0.0035	0.40

COMMUNICATION

p_z	2.9	2.1	2.4	1.8

[a]Spin densities are given as percentages. [b]Total spin density estimated from experimental EPR hyperfine coupling is calculated assuming all spin is located in the orbitals included in the Table. [c]NC = not calculated. [d]All ^{31}P nuclei are equivalent.
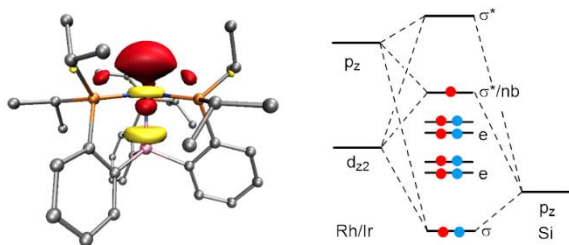

Figure 5. (left) DFT calculated SOMO of [P$_3^{Si}$Rh]$^-$ (**3**) (isovalue = 0.06 a.u.). (right) Qualitative molecular orbital diagram derived from DFT calculated orbital energies and Löwdin reduced orbital spin population analysis. Parent orbitals involved in M. Si bonding shown on either side.

The occupation of an antibonding orbital with significant silicon character represents a particularly unusual case of a 2c/3e$^-$-bond, as silyl ligands are usually regarded as strongly donating.[28] Such strongly donating ligands might be expected to ↑^•˘ |Ó orbitals too destabilized to be populated. The Löwdin reduced orbital spin populations (*vide supra*) give insight into the unusual stability of **3** and **4**. For both complexes, the metal contribution to the SOMO is higher in p_z character than d_z^2 character. This results from symmetry-a‖[¸^åÁ¦àãæ¦Á ãcã*Á-Ác@ÁEÁ ãc@Ác@ÁÇn + 1) s and p_z orbitals of the transition metal. The effect of this mixing has been well-described for both the 2-center, 4-electron case[29] and the 2-center, 3-electron case,[9] as well as in a theoretical study on axial bonding in square planar d^8 ML$_4$ complexes.[30] Here, such {ãcã*Á^•˘|c˘Áã¸Áã^&!^æ^åÁã^•cãã�æã}Á-Ác@ÁEÁ¦àãæ¦Çdue to increased nonbonding character), and we suggest that the P$_3^{Si}$ ligand platform engenders stability in these unusual zerovalent, 2c/3e$^-$ Rh and Ir complexes by striking a balance between &[çæ↑}&˘Áæãåæ&&••ããåãã˘Á-Ác@ÁEÁ¦àãæ¦ÁThe energy of the singly-[&&˘]ãã˘åÁ%æãcã[}ãã˘Áã*Á¦àãæ¦Áã˘ãã¸˘qˆÁㇱ^åÁㆠstrong metal d_z^2. p_z orbital mixing, thus making the M. Si bond more covalent and allowing the electron density to be shared between the two atoms.

As an additional gauge of the importance of covalency in stabilizing complexes **3** and **4**, the electrochemistry of the corresponding P$_3^{Si}$Co(N$_2$) complex was investigated via cyclic voltammetry (see SI). We expected this first-row complex to have the least covalent metal-ligand interactions due to decreased spatial orbital overlap.[31] Indeed, this trend in covalency is observed in a related cationic series [P$_3^{Si}$M(PMe$_3$)][BAr$^F_4$] (M = Co, Rh, Ir; BAr$^F_4$ = tetrakis[3,5-bis-(trifluoromethyl)phenyl]borate)) of divalent metalloradicals we studied previously.[16] For these, the g value of the Co complex (0.61) is significantly larger than that of the Rh and Ir complexes, and the g of the Ir complex (0.33) is slightly larger than that of the Rh complex (0.18), presumably due to the decreased energetic overlap of the metal and ligand orbitals and a larger spin-orbit coupling constant. As mentioned above, this same decrease in covalency moving from Rh to Ir is seen in the present system. Because of the irreversibility of the Co(I/0) redox couple, the $E_{p,c}$ of each complex must be compared, rather than the $E_{1/2}$. While the $E_{p,c}$ of the Rh and Ir complexes appear at ãã]¦[çãæ^|ˆÁ HÈGÀXÈÁc@ÁÁ$E_{p,c}$ of the Co analogue shifts cathodically ¢Á HÈÌÁX (scan rate = 100 mV/s). This shift to a significantly more negative potential is consistent with the

suggested role of metal-ligand covalency in the stabilization of the present zerovalent Rh and Ir complexes.

The metalloradical character of **3** and **4** observed via EPR and corroborated by DFT calculations is manifest in their reactivity with hydrogen; each reacts cleanly with H$_2$ to quantitatively generate the corresponding diamagnetic M(I)-hydride [K(THF)$_3$][P$_3^{Si}$M(H)] (M = Rh (**5**), Ir (**6**)) (Scheme 1) as products of formal H-atom transfer. These complexes were characterized by ^{1}H and ^{31}P nuclear magnetic resonance (NMR) spectroscopy and, in the Rh case, XRD analysis (Figure 6). Despite having a similar structure to **3**, the hydride position of **5** was located in the difference map, and the Rh. K distance increases by over 0.5 Å (see SI for bond metrics). The ^{1}H NMR hydride resonance shown for **5** resembles a quintet, resulting from overlap of a doublet of quartets via coupling of one Rh center and three equivalent P nuclei. This was confirmed by a ^{1}H{^{31}P} NMR spectrum, in which the hydride peak is a doublet. The reactivity of **3** and **4** with H$_2$ is reminiscent of R-H (R = H, alkyl) activations by classic Rh(II) porphyrin metalloradicals.[32]
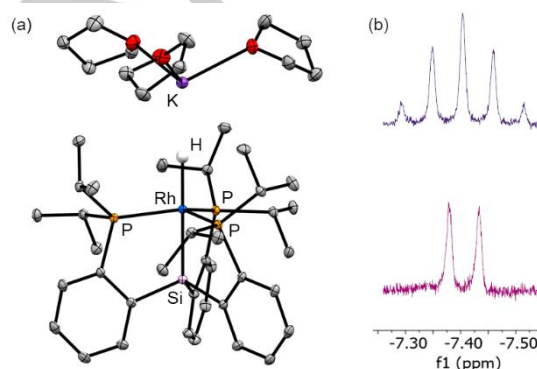

Figure 6. (a) Solid state structure of Rh(I). H **5** derived from H-atom abstraction reactions. Thermal ellipsoids are shown at 50% probability. H atoms (other than the hydride ligand) are omitted for clarity. (b) ^{1}H NMR (top) and ^{1}H{^{31}P} NMR (bottom) of the hydride signal for Rh. H **5**.

To close, the synthesis, isolation, and characterization of zerovalent Rh and Ir complexes bearing 2c/3e$^-$ M. Si bonds has been described. The proposed electronic structure of these complexes, supported by CW and pulse EPR measurements, as well as DFT calculations, are defined by SOMOs that are primarily metal based and considerably stabilized by strong TM d_z^2. p_z orbital mixing. This mixing places substantial spin density on the silicon atom of the silatrane ligand, evinced by ^{29}Si ENDOR spectroscopy. The degree of silicon character in c@ÁE-SOMOs is unusual for TM-silyl complexes, as silyl ligands are strong -donors that lead to highly destabilized antibonding orbitals. Herein, the metal-ligand covalency and buffered destabilization of c@ÁE-orbitals from d. p mixing lead to a rarely observed bonding scheme for a TM-silyl complex.

Acknowledgements

COMMUNICATION
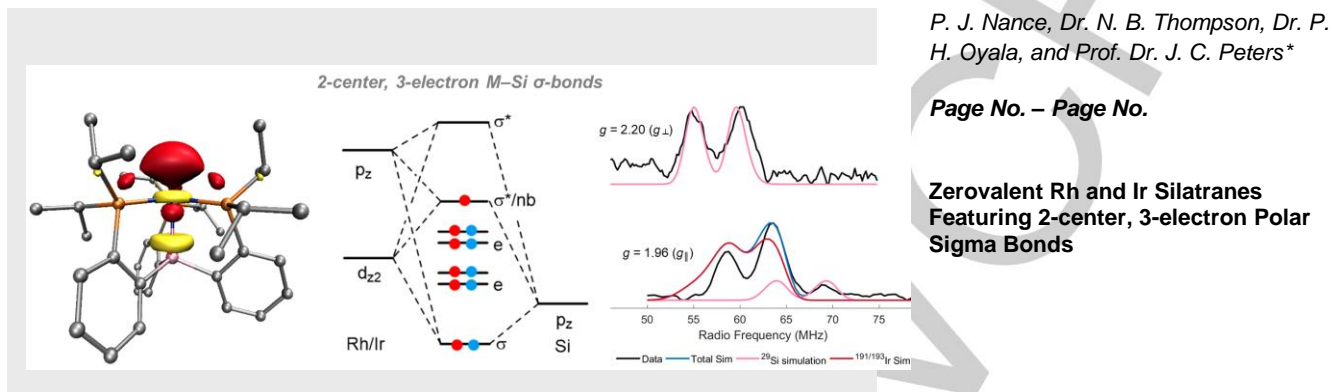
[1] Pauling, L. *J. Am. Chem. Soc.* **1931**, *53*, 3225. 3237.

[2] Castner, T. G.; Känzig, W. *J. Phys. Chem. Solids* **1957**, *3*, 178. 195.

[3] Drews, T.; Seppelt, K. *Angew. Chem. Int. Ed.* **1997**, *36*, 273. 274.

[4] Braïda, B.; Thogersen, L.; Wu, W.; Hiberty, P. C. *J. Am. Chem. Soc.* **2002**, *124*, 11781. 11790.

[5] Alder, R. W. *Tetrahedron* **1990**, *46*, 683. 713.

[6] Gerson, F.; Knoebel, J.; Buser, U.; Vogel, E.; Zehnder, M. *J. Am. Chem. Soc.* **1986**, *108*, 3781. 3783.

[7] Zhang, S.; Wang, X.; Su, Y.; Qiu, Y.; Zhang, Z.; Wang, X. *Nat. Commun.* **2014**, *5*, 4127.

[8] Zhang, S.; Wang, X.; Sui, Y.; Wang, X. *J. Am. Chem. Soc.* **2014**, *136*, 14666. 14669.

[9] Berry, J. F. *Acc. Chem. Res.* **2016**, *49,* 27. 34 and references therein.

[10] Dahl, L. F.; Connelly, N. G. *J. Am. Chem. Soc.* **1970**, *92*, 7472. 7474.

[11] Zheng, X.; Wang, X.; Zhang, Z.; Sui, Y.; Wang, X.; Power, P. P. *Angew. Chem. Int. Ed.* **2015**, *54*, 9084. 9087.

[12] (a) Hofelmeyer, J. D.; Gabbai, F. P. *J. Am. Chem. Soc.* **2000**, *122*, 9054. 9055. (b) Hübner, A.; Diehl, A. M.; Diefenbach, M.; Endeward, B.; Bolte, M.; Lerner, H.-W.; Holthausen, M. C.; Wagner, M. *Angew. Chem. Int. Ed.* **2014**, *53*, 4832. 4835.

[13] Moret, M.-E.; Zhang, L.; Peters, J. C. *J. Am. Chem. Soc.* **2013**, *135*, 3792. 3795.

[14] For select recent references related to 2c/1e⁻ sigma bonds, see: (a) Mierzwa, G.; Gordon, A.; Berski, S. *New J. Chem.* **2018**, *42*, 17096-17114. (b) Oliveira de Sousa, D. W.; Chaer, N.; Marco, A. *Acc. Chem. Res.* **2017**, *50*, 2264-2272. (c) Kusevska, E.; Montero-Campillo, M. M.; Mo, O.; Yanez, M. *Angew. Chem. Int. Ed.* **2017**, *56*, 6788. 6792.

[15] For recently reported complexes featuring 2c/3e⁻-bonding between Ni-Al/Ga, where the three valence electrons are assigned to bonding orbitals, see: Vollmer, M. W.; Xie, J.; Cammarota, R. C.; Young, V. G.; Bill, E.; Gagliardi, L.; Lu, C. C. *Angew. Chem. Int. Ed.* **2018**, *57*, 7815. 7819.

[16] Takaoka, A.; Peters, J. C. *Inorg. Chem.* **2012**, *51*, 16. 18.

[17] Whited, M. T.; Mankad, N. P.; Lee, Y.; Oblad, P. F.; Peters, J. C. *Inorg. Chem.* **2009**, *48*, 2507. 2517.

[18] Boulmaâz, S.; Loss, S.; Schönberg, H.; Deblon, S.; Wörle, M.; Nesper, R.; Grützmacher, H.; Mlakar, M. *Chem. Commun.* **1998**, *23*, 2623. 2624.

[19] Longato, B.; Coppo, R.; Pilloni, G.; Corvaja, C.; Toffoletti, A.; Bandoli, G. *J. Organomet. Chem.* **2001**, *637. 639*, 710. 718.

[20] Longato, B.; Riello, L.; Bandoli, G.; Pilloni, G. *Inorg. Chem.* **1999**, *38*, 2818. 2823.

[21] Schönberg, H.; Boulmaâz, S.; Wörle, M.; Liesum, L.; Schweiger, A.; Grützmacher, H. *Angew. Chem. Int. Ed.* **1998**, *37*, 1423. 1426.

[22] de Bruin, B.; Russcher, J. C.; Grützmacher, H. *J. Organomet. Chem.* **2007**, *692*, 3167. 3173.

[23] Yang, L.; Powell, D. R.; Houser, R. P. *Dalton Trans.* **2007**, *9*, 955. 964.

[24] de Bruin, B.; Hetterscheid, D. G. H.; Koekkoek, A. J. J.; Grützmacher, H. *Prog. Inorg. Chem.* **2007**, *55*, 247.

[25] Schweiger, A.; Jeschke, G. *Principles of Pulse Electron Paramagnetic Resonance.* Oxford University Press: New York, 2001.

[26] Morton, J. R.; Preston, K. F. *J. Magn. Reson.* **1978**, *30*, 577. 582.

[27] DFT parameters in brief: TPSS, ZORA relativistic effect treatment, def2-svp on all atoms except Rh, Ir (def2-qzvp) and Si, P (def2-tzvp). Geometry optimization performed from nuclear coordinates obtained via XRD.

[28] Tilley, T. D. Transition-Metal Silyl Derivatives. In *The Silicon. Heteroatom Bond*; J. Wiley, 1991; pp 245. 308.

[29] Bercaw, J. E.; Durrell, A. C.; Gray, H. B.; Green, J. C.; Hazari, N.; Labinger, J. A.; Winkler, J. R. *Inorg. Chem.* **2010**, *49*, 1801. 1810.

[30] Aullón, G.; Alvarez, S. *Inorg. Chem.* **1996**, *35*, 3137-3144.

[31] Housecroft, C. E.; Sharpe, A. G. *Inorganic Chemistry*, 4th ed.; Pearson: Harlow, 2012.

[32] Wayland, B.B.; Ba, S.; Sherry, A. E. *Inorg. Chem.*, **1992**, *31*, 148. 150.

COMMUNICATION

Entry for the Table of Contents (Please choose one layout)

Layout 2:

COMMUNICATION

P. J. Nance, Dr. N. B. Thompson, Dr. P. H. Oyala, and Prof. Dr. J. C. Peters*

Page No. – Page No.

Zerovalent Rh and Ir Silatranes Featuring 2-center, 3-electron Polar Sigma Bonds

Species with 2-center, 3-electron (2c/3e⁻) -bonds are of interest owing to their fascinating electronic structures and reactivity patterns. Herein we report on a pair of zerovalent (d⁹) trigonal pyramidal Rh and Ir silatranes featuring 2c/3e⁻ -bonds. Structural, spectroscopic, and theoretical data indicate that metal-ligand covalency buffers the expected destabilization of their transition metal (TM)-silyl *-orbitals via d-p mixing, thereby affording distinct examples of polar TM-main group 2c/3e⁻ À@¢ À⁻à[} å• ⁺È